THE JOURNAL OF PHYSICAL CHEMISTRY B

Article

pubs.acs.org/JPCB

# Characterization of Carotenoid Aggregates by Steady-State Optical Spectroscopy

Chen Wang,[†] Christopher J. Berg,[†] Cheng-Chih Hsu, Brittany A. Merrill, and Michael J. Tauber*

Department of Chemistry and Biochemistry, University of California at San Diego, 9500 Gilman Drive MC 0314, La Jolla, California 92093, United States

Supporting Information

**ABSTRACT:** The carotenoids have low-lying triplet excited states and can self-assemble in some solvents to form weakly or strongly coupled aggregates. These qualities make carotenoid aggregates useful for studies of singlet fission, where an outstanding goal is the correlation of interchromophoric coupling to the dynamics and yield of triplet excited states from a parent singlet excited state. Three aggregates of zeaxanthin, two weakly coupled and one strongly coupled, are characterized by steady-state spectroscopic methods including temperature-dependent absorption, fluorescence, and resonance Raman spectroscopy. The absorption spectra for each type of aggregate are distinct; however, an analysis of band positions reveals some important shared characteristics and suggests that the strongly coupled H-aggregate contains a subpopulation of weakly coupled constituents. Temperature-dependent absorption spectroscopy indicates that one of the weakly coupled aggregates can be converted to the other upon heating. The emission spectra of the three aggregates have similar profiles that are overall red-shifted by more than 1000 $cm^{-1}$ relative to the monomer. The emission quantum yields of the aggregates are 5 to 30 times less than that of the monomer, with the lowest yield for the strongly coupled aggregate. The vibrational spectra of the chromophores support only slight perturbations from the structure of solvated monomers. Our findings support the conclusion that all three aggregates are best characterized as H-aggregates, in agreement with a prior theoretical study of lutein aggregates.

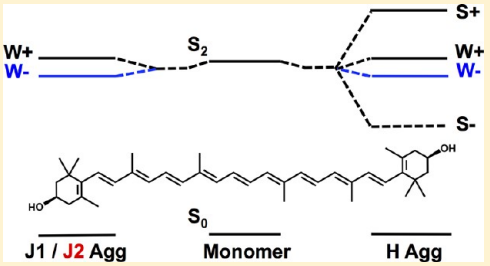


## I. INTRODUCTION

The self-assembly of organic molecular chromophores can lead to new photophysical properties that are not available to the monomer. The photophysics that emerge upon coupling of various chromophores have an impact on applications ranging from photographic science[1,2] to solar energy conversion.[3] In extended systems such as aggregates and thin films, it is well known that subtle changes in preparation conditions can lead to significantly different packing arrangements, and therefore intermolecular interactions, between the molecular constituents. Changes in absorption, emission, and other properties caused by exciton coupling within aggregates have been investigated for numerous chromophores, including cyanines or merocyanines,[4−6] conjugated oligomers,[7−9] xanthenes,[10] acenes,[11] rylene diimides,[12−16] porphyrins/chlorins,[3,17] and carotenoids.[18] Reviews that encompass several classes of dyes or self-assembled systems with mixed chromophores are available.[19,20]

One photophysical mechanism that generally requires the proximity of two chromophores is singlet fission. In this mechanism, a chromophore is photoexcited to its singlet excited state and subsequently partitions its energy over two neighboring chromophores that are both left in triplet excited states. The field of singlet fission has undergone a revival in recent years, in large part because of potential benefit to solar energy conversion.[21,22] An important requirement for efficient fission is that the combined electronic energy of the two triplet excited states be less than that of the parent singlet excited state.[23] As expected, the orientation and coupling strength between chromophores is also important. Theoretical studies have provided some guidance and predictions on the optimal coupling for various classes of chromophores.[22,24] However, there is a shortage of experimental studies that probe the link between fission dynamics and coupling. Ideally, the coupling strength and orientation among a group of chromophores would be varied and correlated with the yield or rate of triplet excited-state formation. Such an approach has been successfully pursued with covalent dimers of tetracene, where low yields of singlet fission have been found for some configurations.[25,26]

Our aim has been to correlate the coupling within assemblies of carotenoids with the dynamics of singlet fission in these systems.[27,28] The chromophore zeaxanthin was selected because its electronic energy levels are favorable for the production of triplet excited states via fission as well as its propensity to aggregate. A high yield of triplet excited states via singlet fission was found for an aggregate of zeaxanthin denoted as J1.[28] The J1-aggregate has a steady-state absorption spectrum that is not strongly red- or blue-shifted relative to the monomer, therefore, the coupling between chromophores is

Special Issue: Richard A. Mathies Festschrift

Received: July 13, 2012
Revised: July 28, 2012
Published: August 9, 2012

  

classified as weak or intermediate.[29] We have also prepared and investigated two other aggregates of zeaxanthin, which we denote J2 and H. The J2-aggregate has an absorption spectrum similar to that of a zeaxanthin aggregate previously reported and labeled as a J-aggregate because of an overall red-shifted absorption spectrum relative to the monomer.[30] Our H-aggregate of zeaxanthin is the same or similar to other strongly coupled blue-shifted aggregates that have been previously reported for zeaxanthin.[30,31]

Optical tools are important for the characterization of aggregates because these samples generally are not amenable to direct structural probes such as X-ray crystallography. We report here the steady-state optical spectroscopy of zeaxanthin aggregates, as background characterization for time-resolved pump−probe absorption and Raman experiments. The methods include absorption and temperature-dependent absorption, continuous-wave (CW) Raman, fluorescence, and circular dichroism (CD) spectroscopy. Several findings are discussed. First, the absorption spectra are easily distinguished and indicate that the aggregates are stable at room temperature for at least several hours. The J1 form is convertible to the J2 upon heating. Second, all three aggregates exhibit similar fluorescence spectra that are red-shifted relative to the monomer. Additionally, the fluorescence quantum yields (QYs) are found to be 5 to 30 times lower than that of the monomer, in contrast with a prior report.[32] Although the H-aggregate primarily consists of strongly coupled chromophores, a weakly coupled subpopulation is suggested by the similarity of its emission profile with those of the other aggregates. Third, our analysis of both the absorption and emission spectra leads to the conclusion that all of the aggregates are best characterized as H-aggregates and that the distinguishing factor is largely the strength, rather than type, of coupling between the constituents. This conclusion agrees with recent theoretical work on aggregates of lutein, which is isomeric with zeaxanthin.[33] Finally, resonance Raman spectra reveal that the structures of the chromophores are very similar in the aggregates and monomer; however, subtle differences in the vibrational spectra suggest slight flattening of carotenoids in the aggregates.

## II. MATERIALS AND METHODS

**Solvents.** Organic solvents (Fisher or Sigma-Aldrich) were spectroscopic-grade and free of stabilizers, or denaturants in the case of ethanol. All were used as received, except tetrahydrofuran (THF), which was passed through an alumina column to remove residual peroxides. Water was deionized with resistivity ≥18 MΩ (Barnstead, model D11911).

**Zeaxanthin.** All-trans 3*R*,3′*R*-zeaxanthin was obtained from DSM Nutritional Products as a 20% (minimum w/w) suspension in corn oil with 1% w/w (±) α-tocopherol. The sample was stored at −80 °C until use. The raw material was washed over filter paper (Whatman, grade 50) with excess hexanes. The solid zeaxanthin was then dissolved in a minimum quantity of acetone at 40 °C and crystallized at −20 °C over an ∼8 h period. The dark-red crystals were filtered, redissolved in acetone and dried by rotary evaporation. The latter step yielded a thin film of zeaxanthin, which facilitated the subsequent dissolution in ethanol (EtOH). The sample was purified by forming aggregates via the reprecipitation method. Water was added 80% (v/v) to the zeaxanthin/EtOH solution, and the zeaxanthin aggregates were collected by passing the solution through a hydrophilic PTFE filter with 0.1 μm pore size (Millipore, Type JVWP). The sample was redissolved in acetone and dried under flowing $N_2$. The purity of the zeaxanthin was confirmed as previously described.[28] The aggregation steps were repeated as needed to obtain consistent preparation of samples for spectroscopic study (described below).

**Preparation of Aggregates.** Three kinds of zeaxanthin aggregates were formed by selecting the conditions for a final reprecipitation step. The H-aggregate (abbreviated as H) formed upon adding 8 mL of water to 2 mL of 50 μM zeaxanthin in EtOH. The J1-aggregate (J1) resulted from adding 9 mL water to 1 mL of 100 μM zeaxanthin in THF. The J2-aggregate (J2) formed with slow addition of 8 mL of water to 2 mL of 50 μM zeaxanthin in 1,4-dioxane. In all cases, the mixing of water and zeaxanthin/organic solutions was done while sonicating (Branson, model 3510) and agitating the receiving vial. Samples were sonicated for an additional 10 min after mixing.

**Transmission Electron Microscopy and Dynamic Light Scattering.** Approximately 15 μL of aggregate solution was applied to a copper grid coated with lacey carbon and settled for 4 min at 4 °C and 100% relative humidity. One drop of 1% uranyl acetate solution was applied to the sample for negative staining to enhance the contrast of the image. Transmission electron microscope (TEM) images were acquired with a FEI Tecnai G2 Sphera microscope with acceleration voltage of 200 KV. The particle size (hydrodynamic diameter) of the aggregates was determined with a dynamic light scattering (DLS) analyzer (JY Horiba, LB-550).

**UV−vis Absorption and Circular Dichroism.** UV−vis absorption spectra of the samples were measured with a scanning spectrometer (Shimadzu, UV-3600). Samples were held in a quartz cuvette with 1 cm path length. The relative extinction coefficient (on a per-monomer basis) of each aggregate sample was determined by filtering zeaxanthin aggregates from each solution, followed by quantitative analysis of the residue by dissolution in ethanol and UV−vis absorption measurements. The procedure yielded relative extinction coefficients that were repeatable within 10% and avoided systematic errors that could result from a propensity of the aggregates to collect at interfaces or settle out of solution. For temperature-controlled experiments, a circulator (PolyScience, 9112A) maintained the temperature of the cuvette to within ±1 °C. Samples for measurements at elevated temperatures were held in a septum-topped cuvette and sparged with $N_2$ prior to heating. After heating and cooling, the sample was dried and redissolved in EtOH, and a UV−vis spectrum was acquired to assess the extent of isomerization. CD spectra were collected with an AVIV model 215 CD spectrometer. Samples were held at room temperature in a quartz cuvette with 1 mm path length. The raw signal was converted to molar CD as described in the Supporting Information.

**Resonance Raman.** The 488.0 nm excitation beam was generated by an argon/Krypton ion laser (Laser Innovations, Innova-70C). The sample solution was flowed through a horizontal capillary with inner dimensions 2 × 2 mm. The excitation power was 0.3 mW. Scattered light was collected at 90° relative to the excitation beam with an F/1.2 camera lens (Canon FD, focal length 85 mm) and focused onto the spectrograph entrance slit with an F/4 achromatic lens. Photons with polarizations parallel and perpendicular to the horizontally polarized excitation beam were collected. A 488.0 nm edge filter (Semrock, RazorEdge) was inserted after the

collection and focusing lenses to reject Rayleigh scattering. A 320 mm focal length spectrograph equipped with a 2400 groove/mm holographic grating and an open-electrode CCD detector (Horiba Jobin-Yvon, iHR-320 and Synapse) were used to disperse and detect the Raman light. The entrance slit width was 50 $\mu$m, and spectral resolution was ~1.7 $cm^{-1}$. Raman shifts were calibrated by acquiring reference spectra of acetonitrile and toluene, which have known peak assignments.[34] The accuracy of the peak positions was ±1 $cm^{-1}$. Solvent peaks were removed from the raw spectra by subtraction of a solvent-only spectrum. Attenuation of Raman scattering caused by absorption of the sample was corrected with an appropriate transmission spectrum. The Raman spectra were also divided by the instrument response of the detection system that was determined by measuring the spectrum of a calibrated white light source (Optronic Laboratory, OL-220C). In a final step, the Raman spectra were smoothed with a Savitzky-Golay algorithm with five-point window.

**Calculations.** Geometry optimization and normal modes of vibration were calculated with density functional theory (DFT) using Gaussian 09W software.[35] The B3LYP functional and 6-31G(d) basis set were employed. The initial geometry of the molecule was taken from crystallographic data of bis[methyl] carbonate zeaxanthin,[36] but with one modification. The torsion angles of the ionone rings around the C6−C7 and C6′−C7′ bonds are different from one another in the crystal, whereas the angles were modified to a single value prior to the calculation to avoid optimization to an asymmetric minimum. The DFT calculation yielded normal modes with real eigenvalues. A scaling factor of 0.961 yielded the best agreement of calculated and experimental Raman frequencies of the strongest bands.

**Fluorescence Spectroscopy.** The fluorescence from the aggregates was too weak, and the scattering too strong for reliable measurement with a commercial fluorimeter. Therefore, the excitation/detection setup for Raman spectroscopy was employed, with changes as noted here. Excitation wavelengths included 457.9, 488.0, and 514.5 nm from the argon/krypton ion laser and 404.3 nm from a blue laser pointer. The power at the sample point was <1.0 mW for each excitation wavelength. Samples were held in a 1 × 1 cm cuvette and had an optical density <0.3/cm at the excitation wavelength. No photodegradation was found by UV−vis absorption at the end of the fluorescence measurements. A polarization scrambler (Opto-Sigma) was placed in front of the spectrograph slit for all measurements. A dichroic polarizer mounted in a rotation stage was positioned between the F/4 focusing lens and scrambler for measurements of the depolarization ratio (see below). The 320 mm spectrograph employed a 600 gr/mm holographic grating, and the slits were adjusted for a spectral resolution of 0.5 nm. Given the low fluorescence emission from the samples, thorough checks for background fluorescence from the optics train were performed. The tests included exchange of antireflection coated optics with those that were uncoated, exchange of various edge or long-pass filters, and checks of the background fluorescence from the optical detection system by replacing the aggregate samples with highly scattering samples of silica.

The fluorescence emission spectra were corrected for the instrument response, as described above. The effect of the sample absorption was corrected using Beer's law to account for two sources of attenuation of the fluorescence emission. First, the raw spectra were divided by a constant (<1) that compensated for absorption of the excitation beam over the ~2 mm excitation path length. Second, the spectra were divided by a spectral transmission function that compensated for absorption of the emission from the sample. The relative amounts of the two types of attenuation depend on specific excitation and emission pathlengths of the 90° scattering setup, and the correction was optimized by monitoring solvent Raman bands of the carotenoid solutions, relative to the same bands of pure solvents. Fluorescence spectra presented on a wavenumber axis were converted from a constant wavelength band-pass to constant wavenumber band-pass by multiplying the emission spectrum by $\lambda^2$. After these corrections, the emission spectra were fitted with multiple Gaussian curves to separate the broad fluorescence emission from the narrow Raman features.

**Determination of Fluorescence Quantum Yields.** The fluorescence QYs $\Phi_F$ of zeaxanthin monomer and aggregates were determined by comparing the intensities of the fluorescence, to Raman bands of an external reference with known Raman scattering cross-section. The derivation outlined in the Supporting Information is modified from the initial report of this technique.[37] We include polarization in our treatment and derive an equation that is analogous to the one reported in prior studies,[38,39]

$$\Phi_F = \frac{8\pi}{3}\frac{N_{Av}}{2303\,\varepsilon}\left(\frac{d\sigma_R}{d\Omega}\right)_{\|+\perp}\left(\frac{c_R}{c}\right)\left(\frac{I_F(\Omega)}{I_R(\Omega)}\right)\left(\frac{1+2\rho_F}{1+\rho_F}\right) \quad (1)$$

where $N_{Av}$ is Avogadro's number, $\varepsilon$ is the decadic molar absorption coefficient, and $(d\sigma_R/d\Omega)_{\|+\perp}$ is the absolute differential scattering cross-section of the reference Raman scatterer. Our reference was EtOH solvent, which was flushed through the same square capillary tubing following measurements of carotenoid monomer in EtOH or carotenoid aggregates in binary water/organic solvent mixtures. The concentrations $c_R$ and $c$ refer to the Raman-scattering reference and to the fluorophore, respectively. $I_F(\Omega)$ is the fluorescence intensity, which is quantified for each recorded emission spectrum by integrating over the broad bands along an energy axis. Similarly, $I_R(\Omega)$ is the intensity of Raman scattering from the reference solvent, integrated over the three prominent C−H stretching bands. The Raman and fluorescence light was collected over the same solid angle ($\Omega$) with the same detection system, which allows cancellation of the detection efficiency and other factors. Scattering and fluorescence with polarizations that are both parallel and perpendicular to the excitation were collected, and spectra were corrected for self-absorption and converted to constant-energy band-pass as described above. The reference value we employ for $(d\sigma_R/d\Omega)_{\|+\perp}$ of ethanol is $35.0 \times 10^{-30}$ $cm^2$/molecule-sr with 488.0 nm excitation, as described in the Supporting Information. The final term in eq 1 accounts for polarization effects, as quantified by the depolarization ratio $\rho = I_\perp/I_\|$. The measured depolarization ratios for the aggregates and monomer deviated 15% or less from 0.33, and this value was used in all calculations of the fluorescence QYs. (See the Results section.)

**Fluorescence Excitation Spectroscopy.** Fluorescence excitation spectra were measured with a xenon arc lamp (Perkin-Elmer Cermax, 175W) in combination with a single-stage monochromator (PTI, 200 mm focal length; with holographic grating from Edmund Optics). Short-pass filters were placed between the monochromator output and the sample cuvette to avoid artifacts from residual light scattering

from the aggregates. The excitation power ranged from 0.02 to 0.17 mW at a spectral band-pass of 5.0 nm, across the 370−540 nm range. The detection setup was as described above. All signals were corrected for variation in the lamp output, as well as attenuation of excitation power by absorption from zeaxanthin.

## III. RESULTS

**Transmission Electron Microscopy.** TEM images of the three types of zeaxanthin aggregates are shown in Figure 1. The aggregates have rod-like shapes with differing dimensions. Representative H-aggregates are ∼50 nm in diameter and 200−300 nm in length, whereas J1-aggregates are typically 20−30 nm in diameter and 500−600 nm in length. The J2-aggregates are much larger, with diameters ∼500 nm and lengths that can exceed 2 μm. The average hydrodynamic diameters inferred from DLS measurement are 200, 100, and 2000 nm for H, J1, and J2 respectively, which are qualitatively consistent with the dimensions determined from the TEM images.

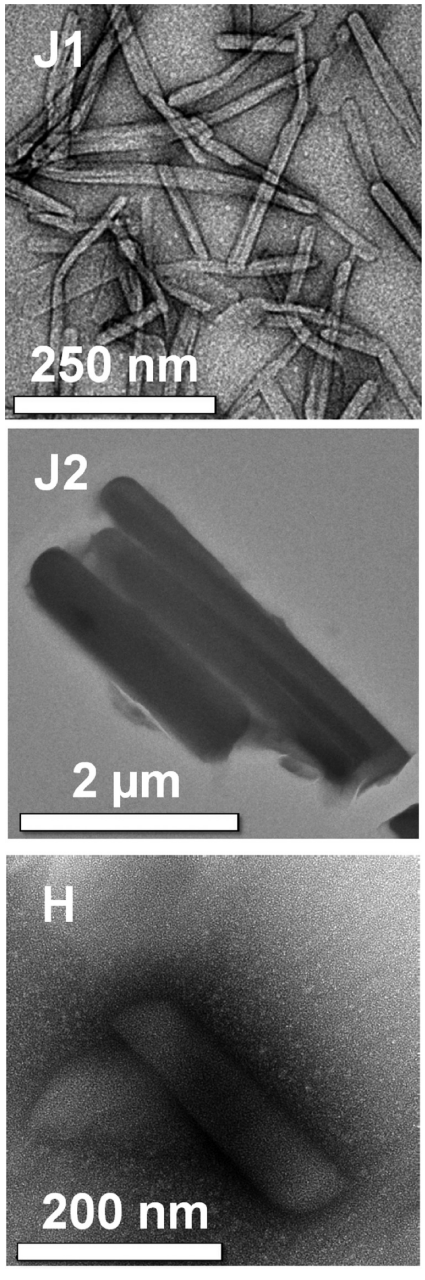


**Figure 1.** TEM images of zeaxanthin J1, J2, and H-aggregates.

**UV−vis Absorption Spectroscopy.** The zeaxanthin aggregates are distinguished from the monomer by their absorption spectra at room temperature (Figure 2A). The spectra are stable for at least several hours. The aggregate solutions showed no sign of residual monomer, as verified by UV−vis analysis of the solution passed through a 0.1 μm filter. The peak extinction coefficients follow the ratio monomer(1.00): J1(0.77): J2(0.65): H(0.79) where all spectra are reported on the basis of equivalent concentration of monomer. The areas under the same spectra, which reflect the oscillator strengths, have a ratio monomer(1.00):J1(0.94):J2(0.94): H(0.70) when integrated on a wavenumber axis from 29 000 to 14 300 $cm^{-1}$. The integrals of the extinction coefficient divided by energy, $\varepsilon(\omega)/\omega$, which are proportional to the square of the transition dipole moments, follow the ratio monomer(1.00):J1(1.00):J2(0.99):H(0.65) over the same integration limits.

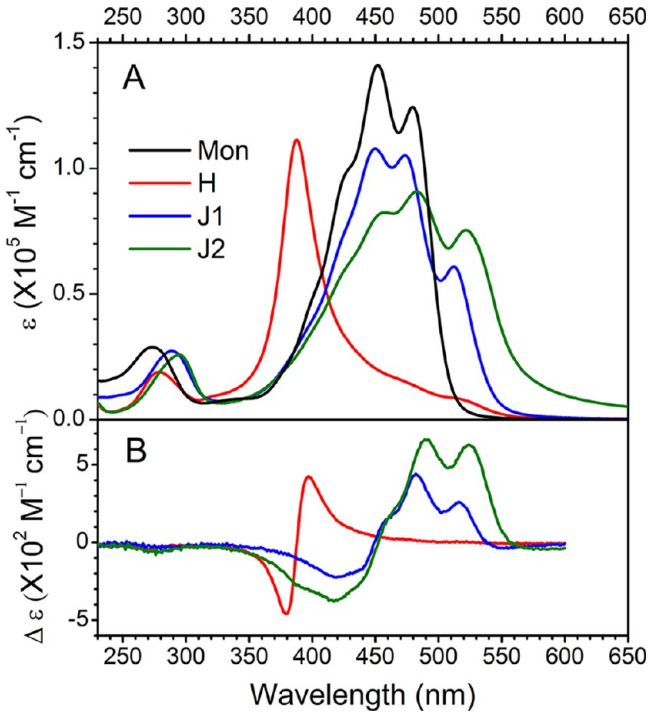


**Figure 2.** (A) UV−vis absorption spectra and (B) circular dichroism spectra of zeaxanthin monomer in EtOH, H-aggregate in 80:20 (v/v) $H_2O$/EtOH, J1-aggregate in 90:10 (v/v) $H_2O$/THF, and J2-aggregate in 80:20 (v/v) $H_2O$/1,4 dioxane.

We now summarize the vibronic features of the zeaxanthin monomer and aggregates. Maxima in the monomer spectrum at 480 and 452 nm are attributed to 0→0 and 0→1 transitions, respectively. These two peaks and two shoulders can be fitted with four Gaussian functions (Figure 3). The three lowest energy bands are separated by ∼1300 $cm^{-1}$, and the fourth band assigned to the 0→3 transition is separated 1500 ± 200 $cm^{-1}$ from the 0→2 band. At higher energy from the visible absorption is a weak band at ∼335 nm, which is a signature of cis-isomers. The small magnitude of this band reflects a minor population of cis-isomers in our zeaxanthin samples. The transition in the ultraviolet ($S_0 \rightarrow S_n$) has a maximum at 274 nm.


dx.doi.org/10.1021/jp3069514 | J. Phys. Chem. B 2012, 116, 10617−10630

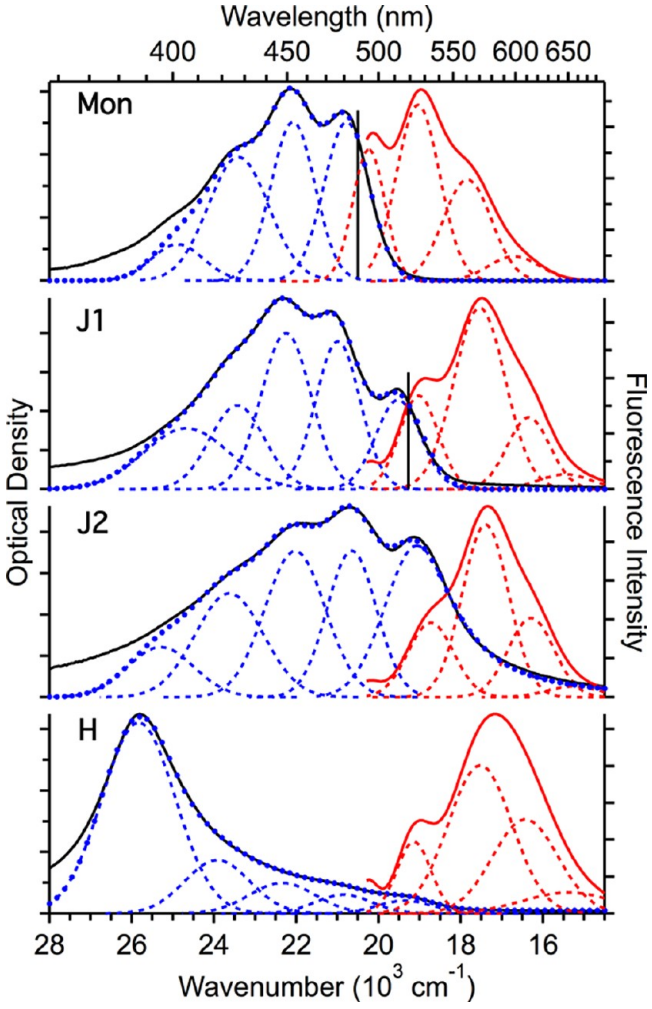


**Figure 3.** Fits to absorption and emission spectra of the zeaxanthin monomer and aggregates. Experimental absorption spectra are solid black lines; fitted Gaussian components are blue dashed lines; and the sum of the components is a blue dotted line. A split half-Gaussian/half-Lorentzian function is used to fit the low-energy wing of J2. Solid red lines depict the broad fluorescence emission profiles, which result from the sum of least-squares Gaussian fits to the experimental 488.0 nm total emission spectra. The Gaussian components are shown as dashed lines; narrow Raman features (Figure 4) are separated in this procedure. The vertical black lines mark the estimated position of the electronic origin, $E_{00}$. The positions of the bands are listed in Table 1.

The spectrum of J1 has three peak maxima located at 513, 474, and 450 nm. The positions are within 1 to 2 nm of those reported for aggregates of zeaxanthin diacetate in 3:1 water/ethanol solution.[40] The three maxima and two shoulders in our spectrum can be fitted with five Gaussian functions. The intervals between centers of neighboring bands, from low to high energy, are 1470, 1260, 1190, and ~1250 $cm^{-1}$. The Gaussian decomposition reveals that the 0→0 band of the J1-aggregate is red-shifted by 1260 $cm^{-1}$ relative to the corresponding band of the monomer. The UV transition of J1 is maximal at 288 nm, which is red-shifted 14 nm (~1800 $cm^{-1}$) relative to that of the monomer.

The J2-aggregate of our study has an absorption spectrum that is similar to a previously classified J-aggregate of zeaxanthin.[18,30] The most prominent maxima of the J2 spectrum are located at 522, 482, and 457 nm, which are red-shifted several hundred wavenumbers relative to corresponding peaks of J1. Four Gaussian functions and one combined half-Gaussian/half-Lorentzian function yield a good fit to most regions of the J2 absorption spectrum (Figure 3, Table 1). The centers of neighboring bands are separated, from low to high energy, by 1590, 1440, 1540, and ~1670 $cm^{-1}$. These intervals are greater than those of J1. The wing of the low-energy band extends much further to the red compared with J1. The wing was fitted with a half-Lorentzian with half-width 1135 $cm^{-1}$. The UV transition for J2 is maximal at ~294 nm, which is red-shifted 6 nm (~700 $cm^{-1}$) relative to that of J1.

The overall spectral profile and maximum at 388 nm of the H-aggregate prepared in our work closely match a prior report of zeaxanthin aggregates in 4:1 water/EtOH.[30] Our spectrum is well-fitted with five Gaussian functions. The center position of the strongest band is blue-shifted approximately 5000 $cm^{-1}$ relative to the peak position of the 0→0 absorption band of the monomer. Several other bands in the spectral range 440−520 nm are also evident. The magnitude of these bands increases with slower addition of water to the ethanol solution of zeaxanthin (Figure S1 in the Supporting Information). The separations between central positions of the fitted bands, from low to high energy, are approximately 1490, 1500, 1580, and 1900 $cm^{-1}$ (Figure 3, Table 1). The UV-band for the H-aggregate is peaked at ~280 nm, which is red-shifted ~6 nm (~780 $cm^{-1}$) relative to the monomer.

The UV−vis spectra of H-, J1-, and J2-aggregates were monitored as the solutions were gradually heated from room temperature to near the solvent boiling point and cooled back to room temperature (Figures S2A and S2B in the Supporting Information). The strong H-aggregate absorption band showed only a small ~2 nm (130 $cm^{-1}$) blue shift that remained after cooling. The bands on the low-energy side of the main peak became more distinct upon heating/cooling and exhibited blue shifts of ~400−600 $cm^{-1}$. The changes in the UV band of H were the most significant in terms of energy; an irreversible ~1500 $cm^{-1}$ hypsochromic shift of the peak position from 278 to 267 nm was found.

**Table 1. Fitted Absorbance and Emission Peaks and Fluorescence Quantum Yields (QYs) of Zeaxanthin Aggregates**

| | absorbance peak positions ($cm^{-1}$) | | | | | emission peak positions ($cm^{-1}$) | | | | fluorescence QY 488.0 nm excitation[b] |
|---|---|---|---|---|---|---|---|---|---|---|
| | peak 5 | peak 4 | peak 3 | peak 2 | peak 1 | peak 1 | peak 2 | peak 3 | peak 4[a] | |
| Mon | N/A | 24900[c] | 23410 | 22080 | 20780 | 20230 | 19040 | 17840 | 16700 | $12 \times 10^{-5}$ |
| J1 | 24690[c] | 23440 | 22250 | 20990 | 19520 | 19020 | 17540 | 16350 | 15460 | $2.5 \times 10^{-5}$ |
| J2 | 25300[c] | 23630 | 22090 | 20650 | 19060 | 18730 | 17400 | 16310 | 15290 | $1.9 \times 10^{-5}$ |
| H | 25820 | 23920 | 22340 | 20840 | 19350 | 19140 | 17530 | 16430 | 15380 | $0.4 \times 10^{-5}$ |

[a]Position and existence of peak 4 in the emission spectra is uncertain. See text for details. [b]Estimated uncertainties in the quantum yields are 10% for the monomer and 20% for the aggregates. [c]Position of these peaks could be subject to ±200 $cm^{-1}$ variation.


dx.doi.org/10.1021/jp3069514 | J. Phys. Chem. B 2012, 116, 10617−10630

The bands of the J1-aggregate change significantly upon heating. The three peak maxima undergo a slight blue shift when first heated to ~60 °C, but the final positions are 200–400 $cm^{-1}$ red-shifted relative to their initial positions after heating to 90 °C and subsequent cooling. The maxima for the annealed J1-aggregate have final positions at 519, 482, and 457 nm, which are nearly identical to the peak positions for unheated J2. Furthermore, the spectrum of J1 after heating and cooling resembles that of the J2-aggregate, with the overall maximum at 482 nm and extended red absorption wing. Upon heating the J2-aggregate solution, the net changes in peak position (~3 nm) are smaller than those observed for the J1-aggregate.

When heated, the zeaxanthin within the aggregate is less likely to isomerize than the monomer in solution, as shown in Figure S3 in the Supporting Information. The dissolution of previously heated J1-, J2-, and H-aggregates revealed weaker bands at ~335 nm, and therefore less cis-isomer formation, than the heated monomeric zeaxanthin in ethanol.

**Circular Dichroism.** Strong optical activity was observed upon aggregation, as shown by CD spectra in Figure 2B. The monomer shows no CD signal in the 350–650 nm spectral region (data not shown), whereas the H-aggregate shows a bisignate couplet that is characteristic of negative and positive Cotton effects. Additional structure is seen for the J1- and J2-aggregates. The amplitudes of the double Cotton effect were observed to decrease nearly 10-fold for H and 4- to 5-fold for J1 and J2, when the solutions were aged for several hours under ambient conditions. The UV–vis spectra remained constant over the same time period. Similar behavior was previously reported.[40]

**Emission Spectroscopy.** The emission spectra of zeaxanthin aggregates and monomer with 488.0 nm excitation are shown in Figure 4. The sharp Raman features of fundamental, combination, and overtone bands of zeaxanthin are prominent in all spectra. The fundamental bands are described further below. The fluorescence spectra of the monomer and aggregates were fitted with a minimum number of Gaussian curves (Figure 3 and Table 1). The emission of the monomer with 488.0 nm excitation has an appearance that resembles a mirror image of the absorption spectrum, in agreement with prior $S_2 \rightarrow S_0$ emission spectra of monomeric $\beta$-carotene and related xanthophylls.[41−46] The emission maximum of the zeaxanthin spectrum in ethanol is located at ~527 nm. The main features of the spectrum can be fitted with three Gaussian functions. The dominant band centered at 19 040 $cm^{-1}$ corresponds to the 0→1 vibronic transition, and two bands are located ~1200 $cm^{-1}$ on either side of the main one. A fourth band at lower energy (~16 700 $cm^{-1}$) is possible; however the lack of an inflection point in the experimental spectrum makes the position and existence of this peak uncertain. The electronic origin $E_{00}$ is estimated to be 20 500 $cm^{-1}$, as derived from the midpoint of the peak maxima for the 0–0 bands of absorption and emission. The $E_{00}$ value found in our work is similar to the values 20 490 ± 460 to 21 010 ± 90 $cm^{-1}$ reported for the $S_0 \rightarrow S_2$ spectral origin of zeaxanthin in EPA, *n*-hexane, or methanol at room temperature.[46]

The emission spectra of all three aggregates are similar to one another, when excited at 488.0 nm (Figures 3 and 4). The spectra all have a maximum in the range 570–585 nm, which is significantly red-shifted relative to the peak of the monomer spectrum. The values measured for $\rho$ at this excitation wavelength were: monomer (0.34); J1(0.36); J2(0.28); and H(0.38). The depolarization ratios of the aggregates were no more than 15% different from a theoretical limit of 0.33 expected for ultrafast emission and parallel transition dipoles for absorption and emission. The variability of $\rho$ within each type of aggregate was not assessed, thus the significance of the deviation from 0.33 is not yet known. Given this uncertainty, a value of $\rho$ = 0.33 was used for the calculation of QYs (eq 1). The dependence of eq 1 on $\rho$ indicates that even if the measured departures from 0.33 for H and J2 were repeatable across multiple samples of these aggregates, the use of the experimental ratios would have only a minor effect on their calculated fluorescence QYs.

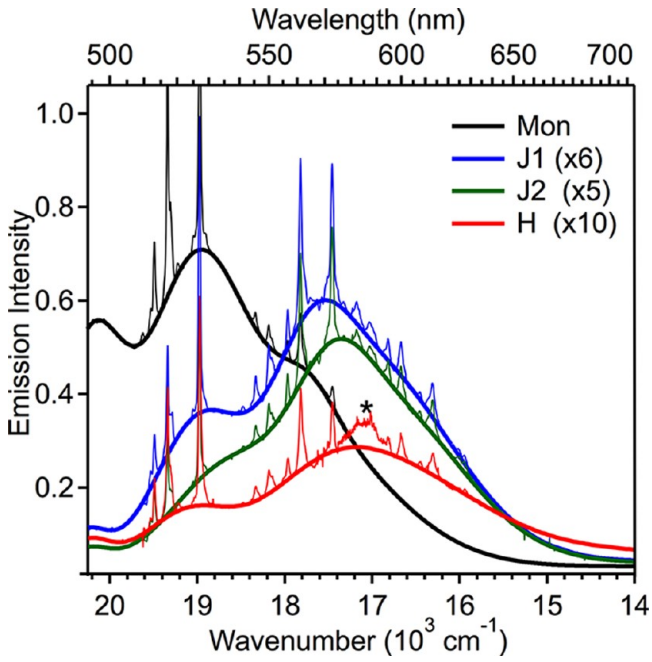


**Figure 4.** Emission spectra of monomeric zeaxanthin (1.0 $\mu$M in EtOH) and aggregates, with 488.0 nm excitation. The experimental spectra are shown as thin solid lines. Sharp features are Raman fundamentals, overtones, and combination bands of zeaxanthin. Spectra of the aggregates are normalized for 1.0 $\mu$M equivalent monomer concentration and scaled as indicated in the Figure. The broad fluorescence component of each experimental spectrum is fitted with four Gaussian functions (see Figure 3). The sum of the Gaussian components is shown as a bold solid line. An asterisk (*) denotes residual Raman scattering from water that remains after subtraction of the solvent-only spectrum.

The aggregate spectra can be decomposed into four Gaussian components. The bluest emission in the region of ~20 000 $cm^{-1}$ is not a clear band and is excluded from the fits reported here. Three bands at highest energy can be assigned for each of the aggregates to vibronic transitions 0→0, 0→1, and 0→2. The dominant band is assigned to 0→1, with central position in the range 17 400–17 540 $cm^{-1}$. The separation between 0→0 and 0→1 bands varies from 1330 to 1610 $cm^{-1}$, depending on the aggregate, but is greater than the monomer in all cases. The separation between 0→1 and 0→2 bands is 1090–1190 $cm^{-1}$, which is similar or smaller than the corresponding separation for the monomer. All fitted peak positions for J1 and H are within 120 $cm^{-1}$ of each other. The peak positions of J2 are red-shifted by 40–290 $cm^{-1}$ relative to those of J1.

The J1 emission spectrum has a mirror-image quality relative to the absorption spectrum. Therefore, an $E_{00}$ value can be estimated from the average of the 0→0 bands of both emission


dx.doi.org/10.1021/jp3069514 | J. Phys. Chem. B 2012, 116, 10617–10630

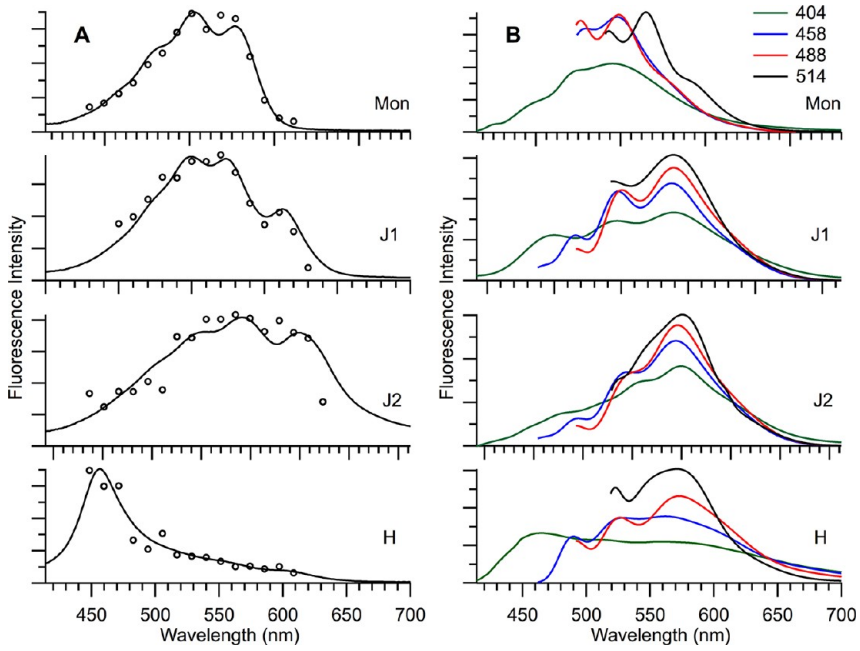


**Figure 5.** (A) Fluorescence excitation spectra of zeaxanthin monomer and aggregates. The excitation spectra each consist of a set of points (open circles) that indicate the emission intensity at 540 (monomer), 605 (J1), 580 (J2), and 630 nm (H). Absorption spectra are shown as black solid lines. The set of emission points for each aggregate is scaled by a factor that is determined by a fit (least-squares) to the corresponding absorption profile. (B) Fitted emission spectra of zeaxanthin monomer and aggregates. The curves are the result of Gaussian fits to the experimental emission spectra (Figure 4 and SI) acquired with four laser excitation wavelengths: 404.3 (green), 457.9 (blue), 488.0 (red), and 514.5 nm (black). Each spectrum is normalized for equal area.

and absorption, as done for the monomer. The value is 19 270 $cm^{-1}$, which is 1230 $cm^{-1}$ smaller than for the monomer. The red shift is nearly the same as the shift of the lowest energy absorption band (1260 $cm^{-1}$). The emission from the J2- and H-aggregates does not have a mirror-image characteristic, thus we do not report $E_{00}$ values for these aggregates.

Excitation spectra (Figure 5A) were acquired to corroborate the source of fluorescence reported in Figure 4. The excitation spectra of the monomer and aggregates largely follow their respective absorption profiles, as expected for pure samples. However, we note that the excitation profile has some dependence upon the wavelength that is monitored, particularly for the H-aggregate. For example, when the monitoring wavelength is 580 nm rather than 630 nm, the normalized excitation profile (not shown) is relatively higher over the range 430−520 nm than predicted from the absorption spectrum. The reason for the variation is that the fluorescence spectrum of the H-aggregate changes with excitation wavelength (Figure 5B). With higher excitation energy, the spectrum broadens, and the emission at the ∼580 nm maximum diminishes more than the intensity at other wavelengths. Similar wavelength dependence in the emission spectra has been noted for monomeric carotenoids.[43,47−50] The broadened emission with higher energy excitation is caused by unrelaxed emission and is discussed further below.

The fluorescence QYs for zeaxanthin monomer and aggregates with 488.0 nm excitation are listed in Table 1. A yield of $12 \times 10^{-5}$ was determined for the monomer in EtOH. Our value is comparable to a previous reported yield of $9.6 \times 10^{-5}$ for zeaxanthin in chloroform;[43] however, it is significantly greater than $4 \pm 2 \times 10^{-5}$ recorded for zeaxanthin in EPA at room temperature.[46] The yields for each aggregate were lower than the monomer: $2.5 \times 10^{-5}$ (J1); $1.9 \times 10^{-5}$ (J2); and $0.4 \times 10^{-5}$ (H). Variability in the aggregate preparation led to changes as high as 20% in the QY. The numbers reported here correspond to reductions in the emission QYs of J1, J2, and H, which are, respectively, 5-, 6-, and 30-fold decreased relative to the monomer. It was also observed that the fluorescence QY of H increases proportionally with the amount of J-type features in its absorption spectrum.

**Raman Spectroscopy.** Resonance Raman spectra of zeaxanthin aggregates reveal that the frequencies of most bands are nearly unchanged relative to the corresponding bands of the monomer (Figure 6 and Figure S5 in the Supporting Information). For example, there are insignificant shifts in the frequency of the C−C single-bond stretch at 1157 $cm^{-1}$ and the methyl rock at 1004−1006 $cm^{-1}$. The structurally sensitive hydrogen out-of-plane (HOOP) modes at ∼870 and ∼965 $cm^{-1}$ have similar frequencies for the monomer and the aggregates. Despite the similarities, small changes in the spectra are apparent. In the ethylenic region, small downshifts are observed upon aggregation, for both the strong band at ∼1520 $cm^{-1}$ and a weak one at ∼1590 $cm^{-1}$. The 1520 $cm^{-1}$ normal mode consists of in-phase stretches of the C═C bonds in the center of the polyene chain, whereas the 1590 $cm^{-1}$ mode consists of in-phase stretches of C═C bonds at the ends of the polyene chain and ionone ring. The extent of the downshift of the main band varies with the excitation wavelength. With 457.9 nm excitation, the downshifts are 8 to 9 $cm^{-1}$ relative to the monomer; with 488.0 nm, 3−5 $cm^{-1}$; and with 568.2 nm, 4−6 $cm^{-1}$. The two J-aggregates show greater downshifts for the ethylenic mode than the H-aggregate. Similar shifts for the zeaxanthin H-aggregate have been previously reported.[31] The downshift of the weak band at 1590 $cm^{-1}$ is similar in magnitude to that of the strong ethylenic band. Finally, we note that a shoulder at ∼1560 $cm^{-1}$ is apparent for the aggregates but not for the monomer.


dx.doi.org/10.1021/jp3069514 | J. Phys. Chem. B 2012, 116, 10617−10630

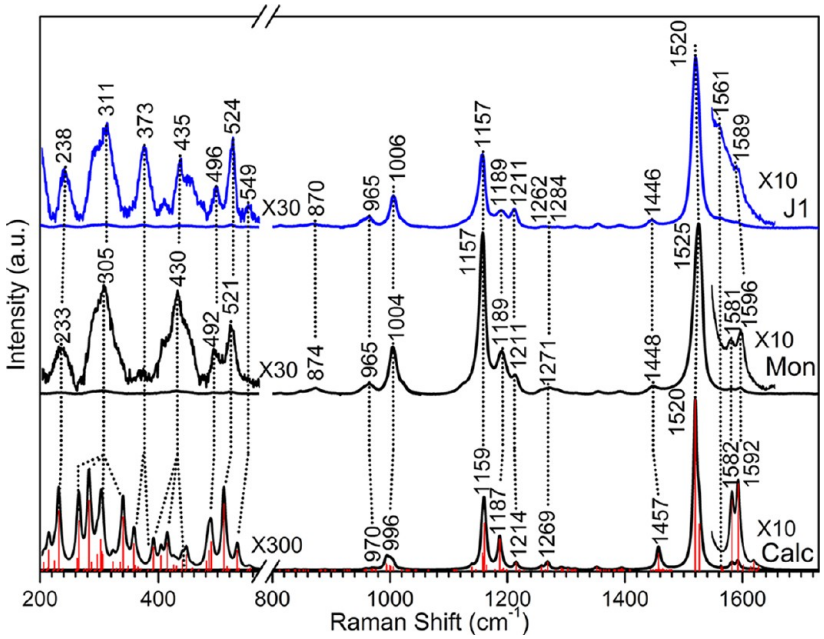


**Figure 6.** Raman spectra with 488.0 nm excitation. (Upper spectrum): zeaxanthin J1- aggregate in 90:10 (v/v) $H_2O$/THF. (Middle spectrum) monomer in EtOH. (Lower spectrum) Calculated vibrations, from DFT optimized structure and after scaling by a single factor to give the best match to the experimental monomer frequencies. (See the text.) The calculated peaks are shown with a 4 cm$^{-1}$ broadening factor. All spectra were normalized to equal peak heights of the ethylenic mode. The 200−570 and 1550−1650 cm$^{-1}$ spectral regions are shown magnified for each spectrum. Labels for the experimental spectra refer to actual maxima of peaks, not fitted. The locations of the maxima for peak shoulders are estimated. Dashed lines guide the eye for corresponding modes among the experimental and calculated spectra. Raman spectra of J2- and H-aggregates are similar to that of J1 (see Figure S5 in the Supporting Information).

Although the frequencies shifts are best characterized as minimal changes, the intensity changes between the monomer and aggregates are noteworthy. First, a 373 cm$^{-1}$ band has stronger Raman activity for all three types of aggregates. Second, the intensity of a vibrational band at 1262−1284 cm$^{-1}$ is significantly smaller for all aggregates relative to the monomer. This band corresponds to a mode with calculated frequency 1269 cm$^{-1}$ and consists of in-plane C−H bond deformations along the polyene chain, in combination with twists of methylene groups of the ionone rings. The intensity of the ∼870 cm$^{-1}$ band diminishes slightly for all aggregates, relative to the methyl rock band at 1004−1006 cm$^{-1}$.

## IV. DISCUSSION

Zeaxanthin forms three different types of nanoparticles that are stable in solution phase at room temperature. These aggregates allow us to probe the effects of interactions between chromophores on optical properties or excited-state dynamics. The exciton coupling within the nanoparticles can be similar to the interactions within thin films or crystals, which makes it worthwhile to compare the aggregates with extended solid-state systems. However, experimental measurements of nanoparticles in solution have several advantages over those of solid-state samples. For example, the absorption or emission spectra of the nanoparticles are measured as readily as their monomeric counterparts. Moreover, the aggregates can be prepared in large batches and flowed, thus facilitating pump−probe spectroscopic measurements (time-resolved resonance Raman and transient absorption spectroscopy) that will be reported elsewhere.

The steady-state optical spectroscopy of the three carotenoid aggregates is the focus of the present work. These spectra probe several characteristics of the aggregates. First, the results from variable-temperature absorption experiments reflect the relative stability of the aggregates. Second, the aggregates have emission QYs that are significantly lower than that of the monomer. Our fluorescence QYs correct a previous report that the emission is significantly higher for zeaxanthin in the aggregated form, relative to the monomer.[32] Third, the emission spectra are similar for all aggregates, which suggests a common exciton structure for the emitting states. Finally, the Raman vibrational data are consistent with prior work[31] showing that the structure of zeaxanthin in the aggregates is similar to that of the solvated monomer. Nonetheless, frequency or intensity changes for the Raman spectra of the three aggregates compared with the monomer allow some insights into subtle structural changes that occur upon self-assembly.

**Formation of Zeaxanthin Aggregates.** Carotenoids form aggregates with significantly blue-shifted (H) and slightly red-shifted (traditionally called J) absorption bands in binary aqueous/organic solvent systems. The blue-shifted spectra are commonly observed for xanthophylls such as lutein, astaxanthin, and zeaxanthin.[18,31,51] Prior studies have highlighted the role of hydrogen bonding among xanthophylls, such as zeaxanthin and lutein, as a factor in the formation of carotenoid H-aggregates.[18,30,51,52] The fact that esterification of xanthophylls, for which H-bonding is impossible, leads to the formation of the J-aggregate rather than the blue-shifted H-aggregate is good evidence of the importance of intermolecular H-bonding.[51−53] Furthermore, the addition of sodium hydroxide to the aqueous component, to pH 10, causes exclusive formation of J-aggregates, presumably because of deprotonation of the −OH groups.[30] Despite the influence of intermolecular hydrogen-bonding in forming H-aggregates, this kind of bonding is not necessary for H-aggregate formation. Examples of H-aggregate formation where intermolecular hydrogen bonding cannot be a factor have been identified, for example,

with the carotenes β-carotene,[54,55] tetradesmethyl-β-carotene,[56] and lycopene.[57]

A full explanation for the differentiation of the aggregates into several types in the present study is not clear. The topic is complex in part because nanoprecipitation is not an equilibrium phenomenon. Previous studies have highlighted the importance of nonequilibrium and kinetic effects.[58] The precipitation of zeaxanthin in water/1,4 dioxane provides a simple illustration. If the 1,4-dioxane solution of zeaxanthin is slowly added to water to a solution 4:1 (v/v) water/ether, then an H-aggregate forms. However, if the water is added to the ether to reach the same solvent ratio, then the J2-aggregate forms. Similarly, the formation of J1- and J2-aggregates in 9:1 water/THF was controlled solely by the rate of the addition of water into the 100 μM zeaxanthin/THF.

On the basis of the present studies of zeaxanthin, we suggest another property, aside from intermolecular H-bonding, that correlates with the outcome of the reprecipitation process. That property is the solubility of the chromophore in the organic solvent. A correlation would be reasonable because solubility is a direct indicator of the strength of chromophore−solvent interactions, relative to chromophore−chromophore interactions. In the reprecipitation process, the replacement of the solvent molecules around each carotenoid by other carotenoids is the first step toward aggregation. We note that zeaxanthin is more soluble in THF than any other organic solvent, with levels ∼20 mg/mL measured in our lab. The solubility of zeaxanthin in 1,4 dioxane is ∼4 mg/mL, which was the second highest among all water-miscible solvents that we tested. Both organic ethers, and particularly THF, tend to form weakly coupled, red-shifted aggregates of zeaxanthin when water is added. We find much lower solubilities of zeaxanthin in ethanol (∼0.1 mg/mL) and acetone (0.5 mg/mL), which are solvents that form strongly coupled H-aggregates. We suggest that the formation of weakly coupled aggregates is correlated with relatively favorable interactions between chromophore and the organic solvent.

**Relative Stability and Surface-to-Volume Ratios of the Zeaxanthin Aggregates.** The temperature-dependence study offers insights into the thermodynamic properties of the aggregates. Whereas heating causes J1 to change irreversibly to J2, the J2-aggregate exhibits only slight changes that partially recover after cooling. Evidently J2 is more stable than J1. The H-aggregate shows small irreversible changes upon heating/cooling. The bands at lower energy from the main peak (see below) are augmented and slightly blue-shifted. The annealing experiments suggest that the J2- and H-aggregate consist of molecules in two stable alignments. We have not found conditions that cause interconversion of H- and J2-aggregates of zeaxanthin. However, astaxanthin assemblies were reported to show evolution between H- and J-aggregates with aging or annealing.[58,59]

The fraction of zeaxanthin molecules located on the surface of the aggregates can be estimated from the TEM images, and crystallographic data for β-carotene, which indicates two molecules in a unit cell of size ∼8 Å × 9 Å × 24 Å.[60−62] Taking J1-aggregate as an example, if a typical aggregate has a cylindrical shape with length 600 nm and diameter 30 nm, then it contains ∼5 × $10^5$ molecules. The length of a zeaxanthin molecule is ∼35 Å. Assuming an average intermolecular separation of ∼4 Å between carotenoids, ∼4 × $10^4$ monomers, or 8%, are located at the aggregate surface. Given that J1 has the smallest volume of the three aggregates, the percentage of molecules at the surface is lower for the other aggregates. The estimate indicates that the vast majority of the zeaxanthin molecules are within the interior of the aggregates, and one would expect that this population largely determines the characteristics of the absorption, Raman, and CD spectra.

**Electronic Transitions and Exciton Coupling in Zeaxanthin Aggregates.** The electronic spectra of monomeric carotenoids with more than nine conjugated double bonds, including β-carotene, lutein, zeaxanthin, and others, are dominated by the symmetry allowed $S_0$ ($1^1A_g^-$) to $S_2$ ($1^1B_u^+$) transition.[63] Although the $S_0 \rightarrow S_2$ absorption is strongly allowed, zeaxanthin and other carotenoids have very low fluorescence QYs on the order of ∼1 × $10^{-4}$ because of ultrafast internal conversion to the dark $S_1$ state.[42,64,65] The $S_2 \rightarrow S_0$ emission spectrum has a mirror-image appearance in comparison with the absorption spectra, as expected for molecules emitting from the same electronic state that is excited. In addition to the $S_2 \rightarrow S_0$ transition, emission from the forbidden $S_1 \rightarrow S_0$ transition is also measurable,[46] but not addressed in the present work.

*Absorption Spectra of H-Aggregate.* The changes in the zeaxanthin absorption profiles upon aggregation are largely a result of exciton-coupling, as previously described for various xanthophylls in binary water-organic solutions.[18,31,33,52,66−69] The H-aggregates are characterized by a strong absorption band that is highly blue-shifted relative to the monomer. The main band is attributed to an allowed transition between the ground state and an in-phase exciton-coupled state. If the exciton-coupling is strong and extends over multiple chromophores, then the absorption bands collapse onto a single, purely electronic transition.[70] The narrow absorption band of the H-aggregate indicates that the exciton is more delocalized for this species than for the J1- and J2-aggregates. The fact that the displacement between the allowed band and the 0−0 band of the monomer is ∼5000 $cm^{-1}$ indicates that the exciton-coupling bandwidth (∼10 000 $cm^{-1}$) is considerably greater than the Franck−Condon bandwidth of the monomer. Therefore, spectra like those reported here for the H-aggregate are clearly in the strong-coupling regime.[33,51,56,70]

The H-aggregate shows substantial decrease (∼30%) in the integral of the extinction coefficient per molecule, relative to unassociated monomer. The loss is known as hypochromism.[71,72] In the case of an exciton-coupled system with a single transition, one would expect that the square of the transition dipole moment, which is proportional to the integral of $\varepsilon(\omega)/\omega$, should be conserved. The finding that the integral is lower for the H-aggregate than the monomer by 35% indicates that the squared transition dipole of this system is diminished. It is likely that coupling to other transitions, combined with the strong interchromophoric interaction for the H-aggregate, are the reasons for the lowered oscillator strength. The theory of hypochromism predicts that the effect should depend on the inverse cube of the distance between chromophores,[71,73] and this distance is expected to be smallest for the strongly coupled aggregate.

Although the nature of the dominant absorption of the H-aggregate is clear, the side bands in the range 420−540 nm need further explanation. An important question regarding these bands is whether they have a physical basis that connects them to the main transition (homogeneous model). Alternatively, the bands could reflect a separate population of molecules (inhomogeneous model). There are several arguments against the homogeneous model. First, none of the

lower-energy side bands is reasonably assigned as an out-of-phase complementary band to the strongly allowed transition. If such a transition were observed for a strongly coupled aggregate, then it would be expected to appear much lower in energy, at approximately 14 000 $cm^{-1}$, when one considers a ~1200 $cm^{-1}$ nonresonant dispersion interaction and symmetric splitting of the allowed and disallowed transitions with respect to the monomer $E_{00}$. Second, the out-of-phase transitions are unlikely to have significant oscillator strength in the case of strong intermolecular coupling.[33] Two pieces of evidence support the inhomogeneous model. First, the fact that the three lowest energy bands of H have peak positions that are within 100−200 $cm^{-1}$ of those of J1 strongly suggests that the physical basis of the bands is the same in both aggregate types, which therefore excludes their close association with the dominant H-band. Next, we note that variation in the mixing speed can change the relative amplitudes of the side-bands, with almost no shift in the peak position of the main H-band (Figure S1 in the Supporting Information). The independent variation of the side-bands again underscores that these transitions exist as a separate phenomenon from the strongly allowed transition of the H-aggregate. In short, the evidence suggests that the H-aggregates have a subpopulation of chromophores that interact in a way similar to those within the J1-aggregate. This subset of chromophores could be small inclusions of J1-aggregates embedded within a matrix of H. Another possibility is that grain boundaries between subsets of the strongly interacting chromophores could give rise to the J1 absorption features.

The present finding of inhomogeneity within zeaxanthin aggregates is in agreement with previous reports for a variety of xanthophylls. For example, aggregates of zeaxanthin, violaxanthin, antheroxanthin, lutein, and other xanthophylls in binary solvents of water/ethanol or water/acetone have spectra with a strong blue-shifted absorption band with peak position <400 nm.[31,68] Other bands in the range 490−520 nm are also evident. The relative magnitude of the <400 nm and 490−520 nm bands generally depends on the specific xanthophyll.[31,68] Similary, violaxanthin aggregates with varying absorption spectra were prepared with two different solvent combinations and experimental procedures.[74]

*Absorption Spectra of J1-Aggregate.* Carotenoid aggregates that have a predominant bathochromic shift have been traditionally termed J-aggregates.[18] We have adopted this nomenclature throughout the present study, but it is important to note that the red-shifted absorption of the carotenoids does not resemble the typical narrow exciton-coupled band of other J-aggregates, such as those formed by some cyanine dyes.[75,76] An alternative explanation for the absorption spectrum of the system denoted in our work as J1 is in terms of a weakly coupled H-aggregate.[33,51] The computational results attribute the ~1200 $cm^{-1}$ red-shifted $E_{00}$ and position of the 0→0 band (relative to the monomer) to nonresonant dispersion interactions.[33] Furthermore, the vibronic intensity pattern of J1, in which the most red-shifted 0→0 band is significantly attenuated relative to 0→2 and 0→3 transitions, is in line with expectations for an H-aggregate.[77] The energy spacings between vibronic transitions of J1 vary from 1470 to 1190 $cm^{-1}$ and have a different pattern from the 1300 $cm^{-1}$ spacing of the monomer absorption. Changes of this kind are expected in the regime where coupling strength is in the range of weak to intermediate.[70,78] Other evidence in favor of assigning the so-called J1-aggregate to a weakly bound H-aggregate is described below, in the context of the emission spectroscopy.

*Absorption Spectra of J2-Aggregate.* The J2-aggregate has absorption features that are very similar to carotenoids in the crystalline state. The optical absorption of crystalline β-carotene has been reported in several studies.[48,62,79−81] The absorption maxima for light with polarization along the long ($b$) axis of the crystal are located at 535, 493, 456, and 426 nm.[81] Similar peak positions have been noted in other studies of crystalline β-carotene[80] and small crystals in solution.[82] The fitted bands for the J2 spectrum have maxima at 525, 484, 453, and 423 nm. The red-shifted 0→0 band relative to the monomer has been long recognized as a characteristic of the crystalline state.[82] To our knowledge, the apportioning of the red-shift to resonant (exciton coupling) interaction versus nonresonant dispersion interactions has not been reported. The red-shifted position for the low-energy absorption of J2 implies that this aggregate is more crystalline-like than the J1. The separations between adjacent peaks of the crystal are 1590, 1650, and 1540 $cm^{-1}$. The first and third values of the separations for the crystal correspond exactly to separations determined for fitted bands of J2. Furthermore, the broad absorption that extends to the red of 600 nm is another connection between the spectrum of the J2-aggregate and the crystal. The origin of this absorption has not been explained in the literature; however, the existence of absorption oscillator strength thousands of wavenumbers red-shifted from the monomer peak must invoke exciton coupling, rather than nonresonant interactions. In summary, the slow mixing process in dioxane/water, or the annealing of the J1-aggregate, leads to a configuration of zeaxanthin molecules that is evidently similar to the state of crystalline β-carotene.

*UV Absorption of the Aggregates.* We address the UV transitions separately from the main band in part because the shifts of this band upon aggregation or change of temperature are sometimes opposite to the shifts in the main band. Specifically, upon formation of the H-aggregate, the UV band *red-shifts* to ~280 nm from the 274 nm peak position of the monomer in ethanol. The direction is opposite to the blue-shifted transition of the main band. Upon heating the H-aggregate, the UV band blue-shifts to 267 nm, whereas the main absorption band at 388 nm remains nearly unchanged. The fact that the UV transition in the H-aggregate shifts in a manner that contrasts with the main band is consistent with a direction and location of the UV transition dipole different from those associated with the main visible transition. It is known that the UV-transition of the carotenoid monomers is largely localized to the extreme ends of the polyene chain, which includes the double bond of the ionone rings in the case of β-carotene and its derivatives.[83] For this reason, the CD signal of monomeric zeaxanthin is restricted to the UV region because the chiral centers at the C3 and C3′ are proximal to the transitions at these ends.[84] Furthermore, a study of the polarized emission from β-carotene agreed with the localization of the UV transition to the ends of the molecule and also found that the transition dipole for the $S_0 \rightarrow S_n$ absorption is shifted 45° relative to the main $S_0 \rightarrow S_2$ transition.[85] Prior to the study of polarized emission in solution phase, an earlier report of the polarized absorption of crystalline of β-carotene had suggested that the UV transition is largely polarized along the short ($a$) axis of the crystal, which is nearly perpendicular to the long axis of the molecule.[79]

A possible explanation for the blue-shift of the UV-band to 267 nm is that heating causes slight translation along the long-axis of molecules that are side-by-side in the H-aggregate. This

small structural rearrangement would likely have little or no effect on the exciton coupling for the main transition dipole that extends along much of the polyene chain. On the other hand, transition dipoles situated near the ionone rings and at an angle 45° turned from the polyene chain would be more sensitive to these specific translations. A blue shift of the UV band in the case of the heated H-aggregate suggests that this "slipping" gives rise to a stronger H-like exciton coupling of these transition dipoles, which overcomes the factors (e.g., nondispersive interactions) that lead to the red shift upon forming the H-aggregate.

*CD Spectroscopy.* Exciton coupling also accounts for the CD of the aggregates in the visible spectral region. The sequence of the positive and negative Cotton effects in the spectra is determined by the chirality of the self-assembled structure, and specifically, the direction of the helix formed by chromophore transition dipoles.[52,86,87] The three aggregates of this study show positive chirality, suggesting that they all form right-handed helical structures. CD signals reflect long-range order and are sensitive to the structure of the aggregate assembly.[33] In our experiments, we have found that the amplitudes of the CD signals decrease over time, whereas the absorption spectra are constant. This observation is consistent with a structural model in which the aggregates are composed of multiple layers.[33,51,52] The diminishment of CD suggests that the interaction between layers may become irregular or decrease over time, whereas intralayer interactions between repeating zeaxanthin units, and hence the absorption spectra, are preserved. An alternative explanation for the decrease in CD is agglomeration of multiple nanoparticles, whereby their optical activity is canceled. Consistent with the latter hypothesis, DLS measurements show that the particle size increases with time.

**Fluorescence Emission.** The aggregate emission spectra are characterized by (1) a significant red shift in the emission relative to the monomer; (2) fluorescence QYs that are a factor of 5 to 30 lower than the monomer; and (3) a pattern of vibronic intensities that is similar for the three aggregates. The emission spectra of the aggregates at room temperature with 488 nm excitation each have a maximum in the range 570−585 nm, and after fitting, the primary band is found to have a central position in the range of 570−575 nm (17 540−17 400 $cm^{-1}$). By comparison, the dominant emission band of the monomer is centered at 525 nm (19 040 $cm^{-1}$). The 1500−1640 $cm^{-1}$ red shift in the emission spectra of the aggregates can be attributed largely to nonresonant dispersion interaction (gas-to-crystal shift). The aggregates exhibit similar spectra relative to one another in terms of both the intensity pattern as well as the separation between vibronic peaks. The ratio of (0→0)/(0→1) band intensities is considerably smaller for the aggregates, relative to the monomer. Furthermore, all of the aggregates show greater separation between the 0→0 and 0→1 transitions (1330−1610 $cm^{-1}$), versus the separation between the 0→1 and 0→2 transitions (1090−1190 $cm^{-1}$). By contrast the monomer has nearly identical (1190 and 1200 $cm^{-1}$) separations between 0→0, 0→1, and 0→2 transitions.

The reduced emission QYs of the three aggregates relative to the monomer are an expected feature for H-aggregates and have a simple explanation in terms of a disallowed transition from the lowest (out-of-phase) exciton-coupled state.[70,88] Furthermore, the changes in the spectral profiles that are described above are characteristic of H-aggregates.[33,77] Recent exciton coupling models have focused on the ratio of the 0→0 and 0→1 transitions in absorption and emission spectroscopy of various organic molecular or oligomer aggregates.[77,89] The 0→0 transition is forbidden in ordered H-aggregates in the theoretical limit of no site disorder; the transition gains intensity as disorder or temperature increases.[77] Aggregates or films of numerous molecular or oligomeric systems, such as oligo(phenylenevinylene), oligothiophene, and MEH-PPV, also show diminished 0→0 bands.[7,9,90−92] In most cases, these systems are considered H-type.

The observation that the fluorescence spectra from H- and J-aggregates are similar to one another is an intriguing result. The approximately mirror-image appearance of the J1 absorption and emission strongly suggests that the emission originates from those exciton-states that are directly excited. As previously mentioned, the low-energy absorption bands of the H-aggregates are best described in terms of a subpopulation of molecules that are weakly coupled. It is likely that these same states are also responsible for the fluorescence emission in the H-aggregates. A heuristic model of the emission from the aggregates is illustrated in Figure 7. The emissive states are depicted as weakly coupled and primarily H-like in character, which is consistent with both the emission pattern and the low QY of fluorescence. The fact that the excitation profile of the H-aggregate corresponds reasonably well to the absorption spectrum, when monitored 630 nm, suggests that energy transfer from the strongly coupled states to the midgap states is relatively independent of excitation wavelength. Furthermore, the relaxation and emission process must occur in <5 ps, as determined by the upper limit from TCSPC measurements (Figure S6 of the Supporting Information). The fast emission additionally provides some evidence that the emission from the aggregates does not simply reflect long-lived trap states that

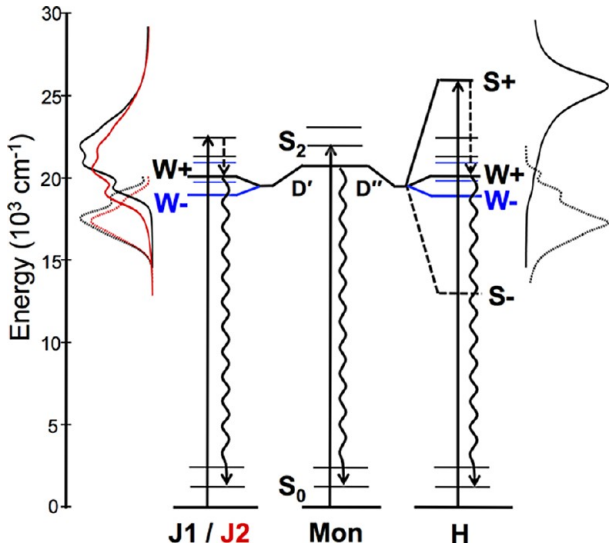


**Figure 7.** Model for the absorption, emission, and nonradiative relaxation processes of zeaxanthin aggregates. Where possible, energy levels are located based on values in Table 1. The aggregate states are qualitatively denoted as weakly (W) or strongly (S) coupled. The (+) and (−) label in-phase and out-of-phase exciton states. Excited vibrational states are indicated by thin lines. D′ and D″ label the shifts in the excited state caused by nonresonant dispersion interactions, or gas-to-crystal shifts, which vary for each aggregate type. Similar interactions for the ground state are not shown.


dx.doi.org/10.1021/jp3069514 | J. Phys. Chem. B 2012, 116, 10617−10630

happen to exist in the aggregates. If these states were to exist, then the emission lifetime would be longer.[93]

There are few reports of fluorescence emission from carotenoids in crystalline form.[80,94] Three bands were reported for $\beta$-carotene crystal at 4 K, at 18 100, 16 900, and 15 770 $cm^{-1}$ (552, 592, 634 nm).[80] The overall mirror-image appearance of emission and absorption spectra allows assignment to the $S_2 \rightarrow S_0$ transition.[80] The 16 900 $cm^{-1}$ (592 nm) band is dominant and is presumably the 0→1 band. The highest energy band at 18 100 $cm^{-1}$ (552 nm) has the smallest amplitude of the three Gaussians, although self-absorption by the crystal may affect the magnitude and position of this peak. The overall pattern of band strengths for low-temperature $\beta$-carotene crystal are similar to that of the aggregates. However, the separation between the 0→0 and 0→1 transitions is 1200 $cm^{-1}$, which is significantly smaller than that of the aggregates. However, it is possible that the position of the 0→0 peak for the crystal could be significantly blue-shifted if reabsorption were not a factor, thus increasing 1200 $cm^{-1}$ to a value that is closer to what we report here for the J2-aggregate.

An additional noteworthy aspect of the H-aggregate is the variation in emission spectrum, as a function of excitation wavelength. This characteristic is certainly not unique to the H-aggregate; analogous character has been described for the $\beta$-carotene monomer.[43,48,49] The fact that the emission of J1 and J2 is less dependent on excitation wavelength is reasonable because in the case of H, additional relaxation processes can occur before the midgap states are populated. The fact that the emission shifts significantly to higher energy with bluer excitation indicates that the nonradiative vibrational or electronic processes occur at a similar rate as the emission itself. Similar conclusions were drawn for the monomer, primarily based on time-resolved fluorescence spectroscopy.

**Molecular Conformation from Resonance Raman Spectra.** The assignments of the vibrational peaks of monomeric carotenoids have been the topic of numerous papers.[95−98] In large part, the mode frequencies of the aggregates are nearly unchanged from those of the monomer, which strongly suggests little perturbation of the monomer structure upon aggregation. Nonetheless, the small changes are ones that reveal subtle, yet important, features of the aggregates.

One of the most obvious changes is the 3−9 $cm^{-1}$ downshifts of the main ethylenic band at ∼1520 $cm^{-1}$. The downshifts are consistent with prior measurements.[31,48] Previous calculations as well as our own reveal that the strong ethylenic $\nu_1$ mode consists of two bands with similar frequencies.[98] Both are dominated by in-phase stretches of C═C modes in the center of the chain. Slight shifts in the peak position of the monomer have been noted upon changing the laser excitation wavelength, and these have been attributed to Raman excitation profiles (REPs) for the two modes that are spectrally shifted relative to one another. However, it is unlikely that the observed differences in ethylenic frequencies for the aggregates can be attributed to shifted REPs for nearby modes, because we see a consistent ordering of downshifts (J2 ≥ J1 > H) for any excitation wavelength in the range 415 to 600 nm. Furthermore, the coincident downshift of the ∼1590 $cm^{-1}$ band, which is associated with a single normal mode, cannot be explained with the REP argument.

It is well known that the C═C bond frequencies downshift as the length of the conjugated region increases. Some researchers have proposed a linear relationship of the main C═C stretching frequency versus $1/(N + 1)$, where $N$ is the number of carbon double bonds.[99,100] Other investigators have suggested empirical downshifts of 3 to 5 $cm^{-1}$ per double bond for chromophores that contain ∼9 double bonds.[101,102] The effective conjugation length of polyenes is affected by its structure. In one scenario, if the ionone rings lie in the plane of the conjugated chain, then the overall extent of conjugation would be significantly enhanced. However, we note that both lutein and zeaxanthin show exactly the same downshift (6 $cm^{-1}$) when comparing the molecules solvated in acetone versus aggregated in 9:1 water/acetone.[31] If the flattening of the rings were the dominant reason for shifts in the ethylenic stretch, then one would expect a decreased effect for lutein because the double bond of one ring cannot be part of the conjugated system. Similarly, astaxanthin and canthaxanthin, which have possible extensions of the conjugation length via the C═O moiety of these molecules, likewise show 5 $cm^{-1}$ downshifts when comparing the acetone-solvated monomers versus aggregates.[31] The conclusion that the downshift in the aggregated state is not primarily a consequence of ionone ring rotation agrees with a previous report.[83] An alternate explanation involves flattening of the polyene chain itself, which also enhances delocalization of the $\pi$ electrons and thus causes downshifts of both the ∼1520 and 1590 $cm^{-1}$ ethylenic modes. This explanation is consistent with the diminished HOOP intensity of the aggregates at ∼870 $cm^{-1}$, which is a sensitive indicator of distortion along the polyene chain.[103,104] The trends in observed downshifts lead to the conclusion that the extent of flattening for zeaxanthin molecules in the aggregates is in the order of J2 > J1 > H.

Additional Raman data suggest that zeaxanthin loses symmetry in the aggregates, possibly because the ionone rings are rotated by unequal amounts out of the plane of the polyene backbone. The out-of-phase C═C stretching modes at ∼1560 $cm^{-1}$ are not expected to be resonantly enhanced when the molecule has a high degree of symmetry. The optimized structure for an isolated zeaxanthin molecule based on DFT calculations shows a symmetric configuration in which the two ionone rings are twisted opposite to one other with matched dihedral angles C5−C6−C7−C8 and C5′−C6′−C7′−C8′ that are ±47°. In the H- and J-aggregates, this symmetry appears to be broken, probably because of intermolecular interactions that may involve the two chiral centers on the ionone rings. Lowered symmetry could cause the out-of-phase 1560 $cm^{-1}$ band to become more intense for the aggregates. Other changes, including the diminished intensity of the 1270 $cm^{-1}$ band (in-phase combination of C−H bending modes) and the increased intensity of the 373 $cm^{-1}$ band (likely a skeletal torsion or CCC bend),[105,106] do not have a clear explanation at this point.

## V. CONCLUSIONS

The present steady-state electronic and vibrational study has been largely motivated by our interest in characterizing carotenoid aggregates for studies of singlet fission.[28] The zeaxanthin aggregates can be reproducibly prepared and are relatively robust, with absorption spectra that are stable for at least several hours. Aggregation is found to hinder isomerization, as compared with monomers in solution. The absorption and emission spectra of the three aggregates are best explained in terms of H-type exciton coupling and distinguished by the strength of the interaction between chromophores. The minor vibrational structural changes that

distinguish monomeric versus aggregated zeaxanthin are slight, and one can therefore conclude that the individual chromophores have similar structures in the three aggregate types. Ongoing work is focused upon the correlation of singlet fission dynamics with exciton coupling and will be reported elsewhere.

## ■ ASSOCIATED CONTENT

### Supporting Information

This material is available free of charge via the Internet at http://pubs.acs.org.

## ■ AUTHOR INFORMATION


### Corresponding Author

*E-mail: mtauber@ucsd.edu.

### Author Contributions

†These authors contributed equally to this work.


### Notes

The authors declare no competing financial interest.

## ■ ACKNOWLEDGMENTS

This material is based on work partially funded by the National Science Foundation (under CHE−1057198), the Hellman Family Foundation, and UCSD start-up support. We acknowledge the use of the UCSD Cryo-Electron Microscopy Facility, which is supported by NIH grants to Professor Timothy S. Baker and a gift from the Agouron Institute to UCSD. We thank the following colleagues for their assistance: Mr. Norman Olson and Ms. Miao-Ping Chien (TEM measurements), Mr. Wei Lin (calculations), Mr. Joseph Taulane (CD spectroscopy), and Mr. Richard Thomas (facilities support). We are grateful for the fluorescence lifetime measurements and helpful input from Professor Douglas Magde, and various valuable contributions from Ms. Maria Angelella and Professor Judy Kim.

## ■ REFERENCES


(1) Reich, C.; Pandolfe, W. D.; Bird, G. R. *Photogr. Sci. Eng.* **1973**, *17*, 334.

(2) Herz, A. H. *Photogr. Sci. Eng.* **1974**, *18*, 323.

(3) McHale, J. L. *J. Phys. Chem. Lett.* **2012**, *3*, 587.

(4) Herz, A. H. *Adv. Colloid Interface Sci.* **1977**, *8*, 237.

(5) Leng, W. N.; Würthner, F.; Kelley, A. M. *J. Phys. Chem. B* **2004**, *108*, 10284.

(6) Rösch, U.; Yao, S.; Wortmann, R.; Würthner, F. *Angew. Chem., Int. Ed.* **2006**, *45*, 7026.

(7) Ostrowski, D. P.; Lytwak, L. A.; Mejia, M. L.; Stevenson, K. J.; Holliday, B. J.; Vanden Bout, D. A. *ACS Nano* **2012**, *6*, 5507.

(8) Peteanu, L. A.; Sherwood, G. A.; Werner, J. H.; Shreve, A. P.; Smith, T. M. *J. Phys. Chem. C* **2011**, *115*, 15607.

(9) Sherwood, G. A.; Cheng, R.; Smith, T. M.; Werner, J. H.; Shreve, A. P.; Peteanu, L. A.; Wildeman, J. *J. Phys. Chem. C* **2009**, *113*, 18851.

(10) Chambers, R. W.; Kajiwara, T.; Kearns, D. R. *J. Phys. Chem.* **1974**, *78*, 380.

(11) Lim, S. H.; Bjorklund, T. G.; Spano, F. C.; Bardeen, C. J. *Phys. Rev. Lett.* **2004**, *92*, 4.

(12) Ahrens, M. J.; Sinks, L. E.; Rybtchinski, B.; Liu, W. H.; Jones, B. A.; Giaimo, J. M.; Gusev, A. V.; Goshe, A. J.; Tiede, D. M.; Wasielewski, M. R. *J. Am. Chem. Soc.* **2004**, *126*, 8284.

(13) Rybtchinski, B.; Sinks, L. E.; Wasielewski, M. R. *J. Am. Chem. Soc.* **2004**, *126*, 12268.

(14) Kaiser, T. E.; Wang, H.; Stepanenko, V.; Würthner, F. *Angew. Chem., Int. Ed.* **2007**, *46*, 5541.

(15) Ghosh, S.; Li, X. Q.; Stepanenko, V.; Würthner, F. *Chem.—Eur. J.* **2008**, *14*, 11343.

(16) Seibt, J.; Dehm, V.; Würthner, F.; Engel, V. *J. Chem. Phys.* **2008**, *128*, 7.

(17) Akins, D. L.; Zhu, H. R.; Guo, C. *J. Phys. Chem.* **1994**, *98*, 3612.

(18) Köhn, S.; Kolbe, H.; Korger, M.; Köpsel, C.; Mayer, B.; Auweter, H.; Lüddecke, E.; Bettermann, H.; Martin, H.-D. Aggregation and Interface Behaviour of Carotenoids. In *Carotenoids*; Britton, G., Liaaen-Jensen, S., Pfander, H., Eds.; Birkhauser Verlag: Basel, Switzerland, 2008; Vol. *4*.

(19) Wasielewski, M. R. *J. Org. Chem.* **2006**, *71*, 5051.

(20) Chen, Z. J.; Lohr, A.; Saha-Moller, C. R.; Würthner, F. *Chem. Soc. Rev.* **2009**, *38*, 564.

(21) Hanna, M. C.; Nozik, A. J. *J. Appl. Phys.* **2006**, *100*, 8.

(22) Smith, M. B.; Michl, J. *Chem. Rev.* **2010**, *110*, 6891.

(23) Paci, I.; Johnson, J. C.; Chen, X. D.; Rana, G.; Popović, D.; David, D. E.; Nozik, A. J.; Ratner, M. A.; Michl, J. *J. Am. Chem. Soc.* **2006**, *128*, 16546.

(24) Greyson, E. C.; Stepp, B. R.; Chen, X. D.; Schwerin, A. F.; Paci, I.; Smith, M. B.; Akdag, A.; Johnson, J. C.; Nozik, A. J.; Michl, J.; Ratner, M. A. *J. Phys. Chem. B* **2010**, *114*, 14223.

(25) Müller, A. M.; Avlasevich, Y. S.; Müllen, K.; Bardeen, C. J. *Chem. Phys. Lett.* **2006**, *421*, 518.

(26) Müller, A. M.; Avlasevich, Y. S.; Schoeller, W. W.; Müllen, K.; Bardeen, C. J. *J. Am. Chem. Soc.* **2007**, *129*, 14240.

(27) Wang, C.; Schlamadinger, D. E.; Desai, V.; Tauber, M. J. *ChemPhysChem* **2011**, *12*, 2891.

(28) Wang, C.; Tauber, M. J. *J. Am. Chem. Soc.* **2010**, *132*, 13988.

(29) Simpson, W. T.; Peterson, D. L. *J. Chem. Phys.* **1957**, *26*, 588.

(30) Billsten, H. H.; Sundström, V.; Polívka, T. *J. Phys. Chem. A* **2005**, *109*, 1521.

(31) Salares, V. R.; Young, N. M.; Carey, P. R.; Bernstein, H. J. *J. Raman Spectrosc.* **1977**, *6*, 282.

(32) Gruszecki, W. I.; Zelent, B.; Leblanc, R. M. *Chem. Phys. Lett.* **1990**, *171*, 563.

(33) Spano, F. C. *J. Am. Chem. Soc.* **2009**, *131*, 4267.

(34) McCreery, R. L. *Raman Spectroscopy for Chemical Analysis*; John Wiley & Sons: New York, 2000.

(35) Frisch, M. J.; Trucks, G. W.; Schlegel, H. B.; Scuseria, G. E.; Robb, M. A.; Cheeseman, J. R.; Scalmani, G.; Barone, V.; Mennucci, B.; Petersson, G. A.; Nakatsuji, H.; Caricato, M.; Li, X.; Hratchian, H. P.; Izmaylov, A. F.; Bloino, J.; Zheng, G.; Sonnenberg, J. L.; Hada, M.; Ehara, M.; Toyota, K.; Fukuda, R.; Hasegawa, J.; Ishida, M.; Nakajima, T.; Honda, Y.; Kitao, O.; Nakai, H.; Vreven, T.; Montgomery, J. A., Jr.; Peralta, J. E.; Ogliaro, F.; Bearpark, M.; Heyd, J. J.; Brothers, E.; Kudin, K. N.; Staroverov, V. N.; Kobayashi, R.; Normand, J.; Raghavachari, K.; Rendell, A.; Burant, J. C.; Iyengar, S. S.; Tomasi, J.; Cossi, M.; Rega, N.; Millam, J. M.; Klene, M.; Knox, J. E.; Cross, J. B.; Bakken, V.; Adamo, C.; Jaramillo, J.; Gomperts, R.; Stratmann, R. E.; Yazyev, O.; Austin, A. J.; Cammi, R.; Pomelli, C.; Ochterski, J. W.; Martin, R. L.; Morokuma, K.; Zakrzewski, V. G.; Voth, G. A.; Salvador, P.; Dannenberg, J. J.; Dapprich, S.; Daniels, A. D.; Farkas, Ö.; Foresman, J. B.; Ortiz, J. V.; Cioslowski, J.; Fox, D. J. *Gaussian 09*; Gaussian, Inc.: Wallingford, CT, 2009.

(36) Linden, A.; Burgi, B.; Eugster, C. H. *Helv. Chim. Acta* **2004**, *87*, 1254.

(37) Champion, P. M.; Lange, R. *J. Chem. Phys.* **1980**, *73*, 5947.

(38) Kochendoerfer, G. G.; Mathies, R. A. *J. Phys. Chem.* **1996**, *100*, 14526.

(39) Tauber, M. J.; Mathies, R. A. *J. Phys. Chem. A* **2001**, *105*, 10952.

(40) Zsila, F.; Bikadi, Z.; Deli, J.; Simonyi, M. *Chirality* **2001**, *13*, 446.

(41) Bondarev, S. L.; Bachilo, S. M.; Dvornikov, S. S.; Tikhomirov, S. A. *J. Photochem. Photobiol., A* **1989**, *46*, 315.

(42) Gillbro, T.; Cogdell, R. J. *Chem. Phys. Lett.* **1989**, *158*, 312.

(43) Jørgensen, K.; Stapelfeldt, H.; Skibsted, L. H. *Chem. Phys. Lett.* **1992**, *190*, 514.

(44) Kandori, H.; Sasabe, H.; Mimuro, M. *J. Am. Chem. Soc.* **1994**, *116*, 2671.

(45) Frank, H. A.; Bautista, J. A.; Josue, J. S.; Young, A. J. *Biochemistry* **2000**, *39*, 2831.

(46) Josue, J. S.; Frank, H. A. *J. Phys. Chem. A* **2002**, *106*, 4815.

(47) Akimoto, S.; Yamazaki, I.; Takaichi, S.; Mimuro, M. *Chem. Phys. Lett.* **1999**, *313*, 63.
(48) Mori, Y. *J. Raman Spectrosc.* **2001**, *32*, 543.
(49) Nakamura, R.; Yamamoto, S.; Nakahara, J. *J. Chem. Phys.* **2002**, *117*, 238.
(50) Nakamura, R.; Wang, P.; Fujii, R.; Koyama, Y.; Hashimoto, H.; Kanematsu, Y. *J. Lumin.* **2006**, *119*, 442.
(51) Zsila, F.; Bikadi, Z.; Keresztes, Z.; Deli, J.; Simonyi, M. *J. Phys. Chem. B* **2001**, *105*, 9413.
(52) Simonyi, M.; Bikadi, Z.; Zsila, F.; Deli, J. *Chirality* **2003**, *15*, 680.
(53) Lematre, J.; Maudinas, B.; Ernst, C. *Photochem. Photobiol.* **1980**, *31*, 201.
(54) Auweter, H.; Haberkorn, H.; Heckmann, W.; Horn, D.; Luddecke, E.; Rieger, J.; Weiss, H. *Angew. Chem., Int. Ed.* **1999**, *38*, 2188.
(55) Horn, D.; Rieger, J. *Angew. Chem., Int. Ed.* **2001**, *40*, 4331.
(56) Okamoto, H.; Hamaguchi, H. O.; Tasumi, M. *J. Raman Spectrosc.* **1989**, *20*, 751.
(57) Wang, L. X.; Du, Z. L.; Li, R. X.; Wu, D. C. *Dyes Pigm.* **2005**, *65*, 15.
(58) Giovannetti, R.; Alibabaei, L.; Pucciarelli, F. *Spectrochim. Acta, Part A* **2009**, *73*, 157.
(59) Mori, Y.; Yamano, K.; Hashimoto, H. *Chem. Phys. Lett.* **1996**, *254*, 84.
(60) Sterling, C. *Acta Crystallogr.* **1964**, *17*, 1224.
(61) Senge, M. O.; Hope, H.; Smith, K. M. *Z. Naturforsch., C: J. Biosci.* **1992**, *47*, 474.
(62) Hashimoto, H.; Sawahara, Y.; Okada, Y.; Hattori, K.; Inoue, T.; Matsushima, R. *Jpn. J. Appl. Phys., Part 1* **1998**, *37*, 1911.
(63) Christensen, R. L. the Electronic States of Carotenoids. In *The Photochemistry of Carotenoids*; Frank, H. A., Young, A. J., Britton, G., Cogdell, R. J., Eds.; Kluwer: Dordecht, The Netherlands, 1999; Vol. *8*, pp 137.
(64) Shreve, A. P.; Trautman, J. K.; Owens, T. G.; Albrecht, A. C. *Chem. Phys. Lett.* **1991**, *178*, 89.
(65) Polívka, T.; Sundström, V. *Chem. Rev.* **2004**, *104*, 2021.
(66) Buchwald, M.; Jencks, W. P. *Biochemistry* **1968**, *7*, 834.
(67) Köpsel, C.; Möltgen, H.; Schuch, H.; Auweter, H.; Kleinermanns, K.; Martin, H. D.; Bettermann, H. *J. Mol. Struct.* **2005**, *750*, 109.
(68) Ruban, A. V.; Horton, P.; Young, A. J. *J. Photochem. Photobiol., B* **1993**, *21*, 229.
(69) Alster, J.; Polívka, T.; Arellano, J. B.; Chabera, P.; Vacha, F.; Psencik, J. *Chem. Phys.* **2010**, *373*, 90.
(70) Kasha, M. *Radiat. Res.* **1963**, *20*, 55.
(71) Cantor, C. R.; Schimmel, P. R. *Biophysical Chemistry Part II: Techniques for the Study of Biological Structure and Function*; W. H. Freeman: San Francisco, 1980.
(72) Parson, W. W. *Modern Optical Spectroscopy*; Springer: Dordecht, The Netherlands, 2007.
(73) Tinoco, I. *J. Am. Chem. Soc.* **1960**, *82*, 4785.
(74) Gruszecki, W. I. *J. Biol. Phys.* **1991**, *18*, 99.
(75) *J-Aggregates*; Kobayashi, T., Ed.; World Scientific: River Edge, NJ, 1996.
(76) Würthner, F.; Kaiser, T. E.; Saha-Moller, C. R. *Angew. Chem., Int. Ed.* **2011**, *50*, 3376.
(77) Spano, F. C. *Acc. Chem. Res.* **2010**, *43*, 429.
(78) Fulton, R. L.; Gouterman, M. *J. Chem. Phys.* **1964**, *41*, 2280.
(79) Chapman, D.; Cherry, R. J.; Morrison, A. *Proc. R. Soc. London, Ser. A* **1967**, *301*, 173.
(80) Gaier, K.; Angerhofer, A.; Wolf, H. C. *Chem. Phys. Lett.* **1991**, *187*, 103.
(81) Hashimoto, H.; Kiyohara, D.; Kamo, Y.; Komuta, H.; Mori, Y. *Jpn. J. Appl. Phys., Part 1* **1996**, *35*, 281.
(82) Shibata, K. *Biochim. Biophys. Acta* **1956**, *22*, 398.
(83) Weesie, R. J.; Merlin, J. C.; Lugtenburg, J.; Britton, G.; Jansen, F.; Cornard, J. P. *Biospectroscopy* **1999**, *5*, 19.
(84) Buchecker, R.; Noack, K. Circular Dichroism. In *Carotenoids*; Britton, G., Liaaen-Jensen, S., Pfander, H., Eds.; Birkhauser Verlag: Basel, Switzerland, 1995; Vol. *1B*.
(85) Bondarev, S. L.; Knyukshto, V. N.; Bachilo, S. M. *J. Appl. Spectrosc.* **2000**, *67*, 88.
(86) Kuhn, H. *Pure Appl. Chem.* **1971**, *27*, 421.
(87) Berova, N.; Di Bari, L.; Pescitelli, G. *Chem. Soc. Rev.* **2007**, *36*, 914.
(88) McRae, E. G.; Kasha, M. *J. Chem. Phys.* **1958**, *28*, 721.
(89) Kistler, K. A.; Pochas, C. M.; Yamagata, H.; Matsika, S.; Spano, F. C. *J. Phys. Chem. B* **2012**, *116*, 77.
(90) Egelhaaf, H. J.; Gierschner, J.; Oelkrug, D. *Synth. Met.* **1996**, *83*, 221.
(91) Clark, J.; Silva, C.; Friend, R. H.; Spano, F. C. *Phys. Rev. Lett.* **2007**, *98*, 4.
(92) Spano, F. C. *Annu. Rev. Phys. Chem.* **2006**, *57*, 217.
(93) Ahn, T. S.; Müller, A. M.; Al-Kaysi, R. O.; Spano, F. C.; Norton, J. E.; Beljonne, D.; Bredas, J. L.; Bardeen, C. J. *J. Chem. Phys.* **2008**, *128*, 11.
(94) Włoch, E.; Więckowski, S.; Turek, A. M. *Photosynthetica* **1987**, *21*, 2.
(95) Saito, S.; Tasumi, M.; Eugster, C. H. *J. Raman Spectrosc.* **1983**, *14*, 299.
(96) Okamoto, H.; Saito, S.; Hamaguchi, H.; Tasumi, M.; Eugster, C. H. *J. Raman Spectrosc.* **1984**, *15*, 331.
(97) Schlucker, S.; Szeghalmi, A.; Schmitt, M.; Popp, J.; Kiefer, W. *J. Raman Spectrosc.* **2003**, *34*, 413.
(98) Tschirner, N.; Schenderlein, M.; Brose, K.; Schlodder, E.; Mroginski, M. A.; Thomsen, C.; Hildebrandt, P. *Phys. Chem. Chem. Phys.* **2009**, *11*, 11471.
(99) Merlin, J. C. *J. Raman Spectrosc.* **1987**, *18*, 519.
(100) Rimai, L.; Heyde, M. E.; Gill, D. *J. Am. Chem. Soc.* **1973**, *95*, 4493.
(101) Koyama, Y. Resonance Raman Spectroscopy. In *Carotenoids*; Britton, G., Liaaen-Jensen, S., Pfander, H., Eds.; Birkhauser Verlag: Basel, Switzerland, 1995; Vol. *1B*.
(102) Ruban, A. V.; Pascal, A. A.; Robert, B.; Horton, P. *J. Biol. Chem.* **2001**, *276*, 24862.
(103) Eyring, G.; Curry, B.; Broek, A.; Lugtenburg, J.; Mathies, R. *Biochemistry* **1982**, *21*, 384.
(104) Curry, B.; Palings, I.; Broek, A. D.; Pardoen, J. A.; Lugtenburg, J.; Mathies, R. Vibrational Analysis of the Retinal Isomers. In *Advances in Infrared and Raman Spectroscopy*; Clark, R. J. H., Hester, R. E., Eds.; Heyden: New York, 1984.
(105) López-Ramírez, M. R.; Sanchez-Cortes, S.; Pérez-Méndez, M.; Blanch, G. *J. Raman Spectrosc.* **2010**, *41*, 1170.
(106) Lin, S. W.; Groesbeek, M.; van der Hoef, I.; Verdegem, P.; Lugtenburg, J.; Mathies, R. A. *J. Phys. Chem. B* **1998**, *102*, 2787.